Computer simulations of localization and quantum transport in a three-dimensional topologically disordered system

Michael K. Gibbons, David E. Logan, and Paul A. Madden
Physical Chemistry Laboratory, University of Oxford, South Parks Road, Oxford OX1 3QZ, United Kingdom
(Received 20 January 1988; revised manuscript received 25 April 1988)

The results of simulation studies of the localization and quantum-transport characteristics of a three-dimensional, off-diagonally disordered tight-binding model are reported. The disorder is characteristic of a hard-sphere fluid, with an exponential transfer-matrix element. The properties calculated include the density of states, the band-edge and mobility-edge trajectories, and the time dependence of the averaged probability, $\bar{P}(t)$, that an excitation will be found at the site at which it was initially located. Localization of eigenstates is inferred from a criterion based on a cutoff in the inverse participation ratio, and an attempt is made to provide a reasoned estimate for the chosen cutoff via time-dependent studies of $\bar{P}(t)$. Pronounced screening effects on the band-edge and mobility-edge trajectories are found and their physical origin is discussed. The consequences of varying the ratio of the hard-sphere diameter to the range of the exponential interaction are investigated. The results obtained for the hard-sphere fluid are contrasted with those for a randomly substituted lattice at the same density.

I. INTRODUCTION

The spatial character of quantum states in disordered materials and the disorder-induced transition between localized and extended eigenstates is a problem of fundamental significance which is relevant to many areas of condensed matter science. In this paper we study by direct simulation the localization and transport characteristics of a three-dimensional system with liquidlike disorder within the framework of a topologically disordered tight-binding model.

Since Anderson's original work,[1] localization has been studied most extensively via a noninteracting tight-binding Hamiltonian on a spatially regular lattice. The matrix element enabling the excitation of interest to transfer from site to site is taken to be nonzero only between nearest lattice neighbors. Randomness is introduced into the Hamiltonian by allowing the site excitation energies to be independent random variables, thereby mimicking the effects of inhomogeneous broadening; and a transition from extended to localized eigenstates occurs when this site-diagonal disorder exceeds a certain critical value. Site-diagonal disorder is, however, somewhat restrictive. In materials such as liquids or amorphous solids a major source of disorder is the randomness in site positions. This results in off-diagonal (or lateral) disorder in which the distance-dependent transfer matrix elements are random variables, reflecting the spatial disorder inherent in the site center-of-mass distribution. When dealing with off-diagonal disorder the macroscopic parameter characterizing the disorder is the number density of active sites ρ, and a transition from localized to extended states occurs when the density exceeds a critical value. Localization with lateral disorder is relevant to the metal-insulator transition occurring in a wide variety of systems ranging from doped semiconductors to liquid metals,[2-4] to the transport of triplet excitons in the impurity band of mixed organic crystals,[5,6] and to the resonant transfer of multipolar Frenkel excitons in liquids.[7,8] In recent years there has been increasing interest in the study of localization in spatially disordered systems by analytical and numerical methods and by direct simulation; see, e.g., Refs. 8–22.

Early simulations of localization with lateral disorder were carried out by Kikuchi[21] and Debney,[22] although their work was limited to fairly small two-dimensional arrays. According to the scaling theory of localization[2,23] there is a fundamental difference between two- and three-dimensional systems: In the former case, all states are predicted to be localized however weak the disorder, whereas for three-dimensional systems a transition from localized to extended states occurs when the disorder is less than a finite critical value. More recently Ching and Huber[20] and Blumen and co-workers[18] have performed direct simulations on a three-dimensional system specified by a tight-binding Hamiltonian with off-diagonal disorder. The active sites were randomly distributed at low occupancy on an underlying lattice, and a transfer-matrix element of exponential form $V(R)\sim\exp(-R/a_H)$ was investigated. Blumen *et al.*[18] studied a system of 100 particles ($N=100$) with 30 configurations ($n_{\rm con}=30$) and with active sites randomly distributed on a simple cubic lattice. Ching and Huber[20(a)] studied an $N=1000$ particle system with $n_{\rm con}=1-2$, using an underlying fcc lattice with 0.01% occupancy; their calculations were later extended[20(b)] to incorporate the effects of overlap into a tight-binding description by examination of an $N=600-700$ particle system with sites distributed at random on a diamond lattice and with a transfer matrix element of modified exponential form. Results were obtained[18-20] for the ensemble-averaged density of states characteristic of the

systems studied and for the inverse participation ratio[24] (IPR) distribution. The localization of eigenstates was inferred from the IPR by choosing somewhat arbitrarily a finite lower bound such that states of given energy with an IPR greater (less) than the cutoff value are considered to be localized (extended). By performing a range of simulations with a fixed density ρl^3 of active sites, and by varying the ratio a_H/l (where a_H is the range of the exponential interaction and l the lattice constant), Ching and Huber[20(a)] demonstrated the existence of a mobility edge between localized and extended eigenstates, and estimated the critical a_H/l associated with the disappearance of extended states.

In this paper we also study a three-dimensional laterally disordered tight-binding model with a simple exponential transfer-matrix element. In contrast to Refs. 18–20 we focus on a system with liquidlike disorder: the random site distribution is generated by quenching center-of-mass configurations characteristic of a hard-sphere fluid at the chosen number density. Calculations are typically performed with 12 configurations of 500 particles, although results with N up to 2000 are also reported in an effort to investigate some system size effects. Use of a hard-sphere system together with an exponential transfer-matrix element produces two characteristic length scales, σ and a_H, where σ is the hard-sphere diameter such that no two sites can be separated by a distance less than σ.

In Sec. II we describe the calculational procedures employed and examine the averaged density of states for a range of both reduced density $\rho^*=\rho\sigma^3$ and the ratio σ/a_H. We also discuss theoretically the form of the density of states as appropriate to low densities at or near the upper edges of the band where pair states predominate, and compare the predictions with our computational results. The computed density of states is also compared with that resulting from a substitutionally disordered system with active sites distributed at random on an underlying lattice.

In Sec. III we examine the localization characteristics of the system. Localization of eigenstates is inferred from the IPR, and in Sec. III we choose and proceed with an IPR cutoff of 0.16 as a boundary between "localized" and "extended" eigenstates. An attempt to justify this cutoff via timescale arguments will be given in Sec. IV. With the chosen IPR criterion we estimate the critical number density required for all states in the band to become localized (the Anderson transition density). We also estimate mobility-edge and band-edge trajectories for the system, i.e., how the mobility edges and band edges in the density of states vary with density for a given σ/a_H. Strong asymmetry is observed in both. For a given density, localized states in the upper half-band are more strongly localized than states in the lower half-band. In fact, states in the lower half-band are localized only weakly at best, and the clear existence of a lower mobility edge is difficult to ascertain, as was also observed by Ching and Huber[20] and by Debney.[22] We suggest in Sec. III that this behavior may be understood, at least in part, in terms of the notion of transfer-matrix element screening.[16] We also discuss briefly in this section the effective "radius of gyration," R_α, of an eigenstate, which gives a measure of the spatial extent of an eigenstate of given energy.

In Sec. IV we consider an "experiment" in which an excitation is created at time $t=0$ on a specific site i. The probability $P_{ii}(t)$, that the excitation will be found on site i again at time t can be expressed in terms of the eigenvalues and eigenvector coefficients of the tight-binding Hamiltonian calculated in Secs. II and III. The time dependence of the ensemble-averaged probability $\bar{P}(t)$ can, therefore, be calculated. A wide range of information can be extracted from such studies. One example is given in Sec. IV. We examine for a finite-size system the long time contributions to $P_{ii}(t)$ arising from eigenstates of the system which could be considered as localized and those which could be regarded as extended. We argue that only the latter can effectively contribute to the observed long time delays in $\bar{P}(t)$, and for $N=500$ particle systems are thereby able to estimate an acceptable IPR cutoff separating localized from extended eigenstates of the system.

II. DENSITY OF STATES

For a fixed center-of-mass configuration $\{\mathbf{R}_i\}$ the quantum mechanics of the system is specified by a tight-binding Hamiltonian,

$$\hat{\mathcal{H}}=\sum_i |i\rangle\epsilon_i\langle i| + \sum_{ij}{}' |i\rangle V_{ij}\langle j| \ , \tag{1}$$

where the sum runs over all sites. In this paper we are interested in pure lateral disorder. In the absence of site-diagonal disorder $\epsilon_i=\epsilon$, and we take $\epsilon=0$ without loss of generality. We study a simple exponential transfer-matrix element

$$V_{ij}=-V_0\exp(-R_{ij}/\alpha_H) \ , \tag{2}$$

where $R_{ij}=|\mathbf{R}_i-\mathbf{R}_j|$. For a given configuration the eigenstates of $\hat{\mathcal{H}}$ are denoted by $|\Psi_\alpha\rangle$ with a corresponding energy E_α. The $|\Psi_\alpha\rangle$'s may be expanded as

$$|\Psi_\alpha\rangle=\sum_i C_{i,\alpha}|i\rangle \ , \tag{3a}$$

where

$$\sum_i C^*_{i,\alpha}C_{i,\beta}=\delta_{\alpha\beta} \ , \tag{3b}$$

$$\sum_\alpha C^*_{i,\alpha}C_{j,\alpha}=\delta_{ij} \ , \tag{3c}$$

as both the eigenvectors $\{|\Psi_\alpha\rangle\}$ and the site basis $\{|i\rangle\}$ form orthonormal sets.

Quenched configurations of a hard-sphere fluid at a specified reduced density ρ^* were generated by standard methods. Periodic boundary conditions were employed, consistent with which a minimum image convention was used such that sites separated by more than half of the basic cell length L did not interact. Unless stated to the contrary, the results reported refer to calculations with a basic cell containing $N=500$ particles. Eigenvalues and eigenvectors of the Hamiltonian Eq. (1) were obtained by complete diagonalization. More precisely we obtain the

eigenvalues $\tilde{E}_\alpha = E_\alpha / V_0$ of the matrix $M_{ij} = (1-\delta_{ij}) V_{ij} / V_0$, so that all eigenvalues are quoted in units of V_0. Most calculations were performed for the ratio $\sigma / a_H = 0.9$ (which will be implicit unless stated otherwise), although the variation in our results with σ / a_H will also be discussed.

The computed $\tilde{E}_\alpha$ give directly the density of states (DOS) for a given configuration. In Fig. 1 we show the averaged DOS per site [such that $\int_{-\infty}^{\infty} D(\tilde{E}) d\tilde{E} = 1$] obtained as an average over 12 configurations, and for the three reduced densities $\rho^* = 2 \times 10^{-3}$ ($\rho a_H^3 = 2.74 \times 10^{-3}$), 10^{-2} ($\rho a_H^3 = 1.37 \times 10^{-2}$), and 5×10^{-2} ($\rho a_H^3 = 6.86 \times 10^{-2}$). The DOS is smoothed by averaging over an energy interval large enough to give adequate statistics and small enough to preserve detail, with resultant points fitted by a cubic spline. For sufficiently low number density the DOS is symmetric in energy about the unperturbed site energy $\tilde{E} = 0$, with a large central peak. As ρ^* is progressively increased the DOS acquires a characteristic and familiar asymmetry with an increasingly long tail in the lower half-band and with the DOS maximum shifted progressively into the upper half-band.

The ensemble averaged DOS, $D(E) = D(\tilde{E}) / V_0$, is given by

$$D(E) = -\pi^{-1} \langle \mathrm{Im} G_{ii}^{+}(E) \rangle \ , \tag{4}$$

where $G_{ii}^{+}(E) = \lim_{s \to 0+} G_{ii}^{+}(E + is)$, and $G_{ii}(z)$ is the diagonal element of the Green function $G_{ij} = \langle i \mid (z - \hat{H})^{-1} \mid j \rangle$ for the tight-binding Hamiltonian, which from Eq. (1) satisfies

$$z G_{ij}(z) - \sum_k{}' V_{ik} G_{kj}(z) = \delta_{ij} \ . \tag{5}$$

Equations (4) and (5), together with the hard-sphere distribution function, form a basis from which analytical approximations to the DOS may be developed. Most work in this area has been concerned with a perfectly random spatially disordered system corresponding to the $\sigma = 0$ limit, e.g., the Matsubara-Toyozawa approximation[25] and its modification,[26–28] although Katz and Rice[29] have developed approximate methods for taking the hard-sphere structure into account. The above theories, however, are not appropriate[30] in the low density range over which we expect appreciable persistence of localized states (ρa_H^3 less than ~ 0.01–0.03), which is the density domain of primary interest in this paper. A description of the DOS has been developed by Elyutin[30] which is valid in the density range $10^{-2} \gtrsim \rho a_H^3 \gtrsim 10^{-3}$ for the $\sigma = 0$ case of a perfectly random system. We now discuss briefly this approach, as there are several features of it which are relevant both to the averaged DOS and the localization problem.

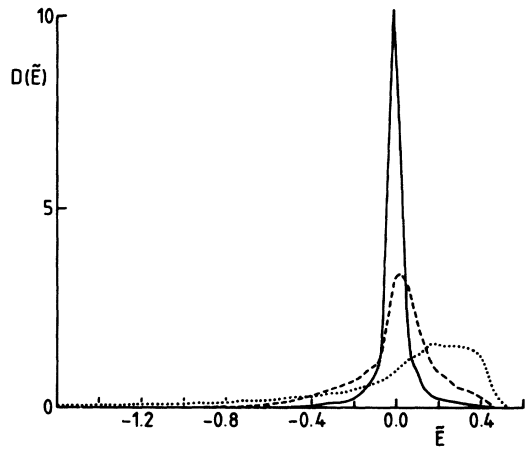

FIG. 1. The averaged density of states, from 12 configurations of 500 particles, for $\sigma / a_H = 0.9$, and at reduced densities of $\rho^* = \rho \sigma^3 = 0.002$ (solid line), $\rho^* = 0.01$ (dashed line), and $\rho^* = 0.05$ (dotted line).

For a given realization of the system, the self-energy $S_i(z)$ of atom i is defined through the inverse of the diagonal Green's function by

$$G_{ii}(z) = [z - S_i(z)]^{-1} \ . \tag{6}$$

Equation (5) may be employed to generate a renormalized perturbation series[31] (RPS) for the self-energy, which takes the form

$$S_i = \sum_{j(\neq i)} \frac{\mid V_{ij} \mid^2}{(z - S_j^{(i)})} + \sum_{j(\neq i)} \sum_{k(\neq i,j)} \frac{V_{ij} V_{jk} V_{ki}}{(z - S_k^{(i,j)})(z - S_j^{(i)})} + \cdots \ . \tag{7a}$$

Here, terms such as $S_j^{(i)}$ represent the self-energy of site j in a system with site i removed and are defined by a series analogous to Eq. (7a) but with the appropriate site(s) excluded from the sum. Truncation of the RPS at the second-order term gives

$$S_i(z) \simeq \sum_j{}' \frac{\mid V_{ij} \mid^2}{z - S_j^{(i)}(z)} \ . \tag{7b}$$

Equation (7b) may be iterated, and leads via Eqs. (4) and (6) to an approximate result[30] for $D(E)$. At this level the DOS is necessarily symmetric in energy about $E = 0$: Asymmetry in $D(E)$ arises[16,30] from irreducible $m \geq 3$-body terms in the RPS, Eq. (7a), which are neglected in Eq. (7b). The procedure sketched is equivalent to a resummation of all (averaged) interaction graphs contributing to $D(E)$ which have the topology of Cayley trees with variable connectivity;[30] the resultant expression for $D(E)$ is valid for $\sigma = 0$ in the low ρa_H^3 domain. Elyutin finds[30] that the band edge in the DOS is given by

$$\tilde{E}_+ = 1 + O(\rho a_H^3) : \sigma = 0, \quad \rho a_H^3 \to 0 \tag{8a}$$

and that in the outer edges of the band ($1 \gtrsim \tilde{E} \gg 0$) the functional form of the DOS is

$$D(\tilde{E}) = 2\pi \rho a_H^3 \frac{(\ln \mid \tilde{E} \mid)^2}{\mid \tilde{E} \mid} \ . \tag{8b}$$

Equations (8) refer to the $\sigma = 0$ limit. However, we can generalize to the case of finite σ, and gain some physical insight into the origins of (8), if we assume that at sufficiently low density the wings of the band reflect the distribution of bonding and antibonding interactions as-

sociated with interacting *pairs* of sites. We solve Eq. (5) trivially for an $N=2$ particle system and perform an ensemble average to give

$$D(E)\simeq\rho\int d\mathbf{R}\,\tfrac{1}{2}[\delta(E+V(R))+\delta(E-V(R))]g_0(R)\ , \tag{9a}$$

where $g_0(R)$ is the radial distribution function for a hard-sphere fluid. We expect Eq. (9a) to be reasonable towards the wings if indeed that region is dominated by pair interactions. The $\rho\to 0$ limit of $g_0(R)$ is the step function $\Theta(R-\sigma)$; higher-order density terms in a virial expansion of $g_0(R)$ give a negligibly small contribution to (9a) in the density range of interest and do not alter the position of the predicted band edges. For the exponential $V(R)$, Eq. (2), together with $g_0(R)=\Theta(R-\sigma)$, Eq. (9a) can be simplified to

$$D(\tilde{E})=V_0D(E)$$

$$\simeq 2\pi\rho a_H^3\int_0^\beta dx\frac{(\ln x)^2}{x}[\delta(x-\tilde{E})+\delta(x+\tilde{E})]\ , \tag{9b}$$

where $\beta=\exp(-\sigma/a_H)$. This simple calculation therefore predicts the band edge to occur at

$$\tilde{E}_+=\exp(-\sigma/a_H) \tag{10}$$

which for $\sigma=0$ reduces precisely to the leading term in (8a). In physical terms the diminution of $\tilde{E}_+$ from unity reflects the existence of a minimum site separation σ, so that the maximum $|V(R)|/V_0$ is reduced from 1 to $e^{-\sigma/a_H}$. From (9b) the DOS is also predicted to have precisely the form (8b) within the band $[|\tilde{E}|\leq\exp(-\sigma/a_H)]$.

The analysis leading to Eqs. (9) and (10) is trivial, but it gives some insight into the nature of states near the edges of the band at low density and reveals the physical origin of Eq. (8). It suggests that if the observed DOS near the upper and/or lower edges of the band conforms to Eq. (8b), then states in that region are largely due to pair states which we would expect to be spatially localized. This will be discussed further in the following section. In Fig. 2 we compare Eq. (9b) with the computed $D(\tilde{E})$ (for $N=1000$, $n_{\rm con}=6$) at $\rho^*=2\times10^{-3}$ and with $\sigma/a_H=0.9$ $[\exp(-\sigma/a_H)\simeq 0.41]$. As is seen from the figure the agreement is quite reasonable at this density for $|\tilde{E}|\gtrsim 0.07$. The effect of varying σ/a_H is illustrated in Fig. 3 where we plot $D(\tilde{E})$ for a fixed $\rho a_H^3=6.9\times10^{-3}$ and with $\sigma/a_H=0.7$, 1, and 1.3. The DOS has a degree of asymmetry at this density, but if states towards the *upper* edge of the band are due primarily to pair interactions we would expect from Eqs. (8a) and (10) that $\tilde{E}_+$ would be given by $\tilde{E}_+=\exp(-\sigma/a_H)+c\rho a_H^3$, where the coefficient c depends on σ and reduces to $c=3.78$ (Ref. 30) for $\sigma=0$. We see from Fig. 3 that in each case the DOS in the upper-density decays to zero at a value close to and slightly greater than $\exp(-\sigma/a_H)$.

We now refer briefly to the asymmetry in the DOS observed in Fig. 1 at the higher densities $\rho^*=0.01$ and 0.05. As mentioned previously the asymmetry in $D(E)$ arises from the irreducible $m\geq 3$-body terms in the RPS, Eq. (7a). Logan and Wolynes[16] have developed a simple method of incorporating higher-order RPS terms into a self-consistent theory of both localization and the averaged DOS. Within their formulation, Eq. (7a) is replaced by $(s\to 0+)$

$$S_i(E+is)\simeq\sum_j{}'\frac{|\Phi_{ij}(E)|^2}{E+is-S_j^{(i)}(E)}\ . \tag{11}$$

Equation (11) is of precisely the form (7b) which results from truncating the RPS at the second-order term, but with the bare transfer-matrix element V_{ij} replaced by an energy-dependent renormalized transfer-matrix element $\Phi_{ij}(E)$. The effective transfer-matrix element takes account of the higher-order terms in the RPS in a simple mean-field sense and, physically, reflects the screening of the interaction between a pair of sites by the other sites in the system. With a Yukawa transfer-matrix element

$$V(R)=-(V_0/R)\exp(-R/a_H^0)\ ,$$

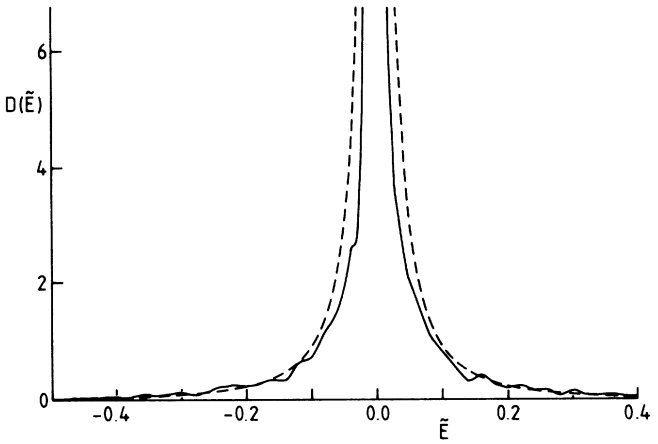

FIG. 2. A comparison between the computed DOS at $\rho^*=0.002$ with $\sigma/a_H=0.9$, and the band-edge behavior calculated from Eq. (9b).

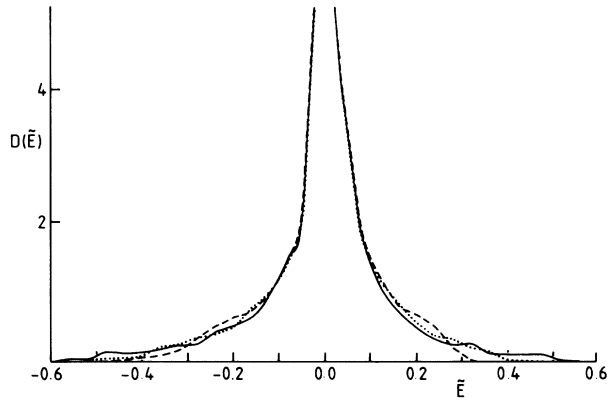

FIG. 3. The effect of varying σ/a_H on the DOS at the constant reduced density $\rho a_H^3=0.0069$; $\sigma/a_H=0.7$ (solid line), $\sigma/a_H=1.0$ (dotted line), $\sigma/a_H=1.3$ (dashed line).

Logan and Wolynes find[16] that the renormalized $\Phi(R,E)$ takes the same form as the bare $V(R)$ but with a_H^0 replaced by an energy-dependent decay length $a_H(E)$. For $E>0$ ($E<0$) it is found that $a_H(E)<a_H^0$ [$a_H(E)>a_H^0$]. The effective transfer matrix element is thus of shorter (longer) spatial range than the bare $V(R)$ for states in the upper (lower) region of the band. As discussed in Ref. 16 it is this feature which gives rise both to asymmetric tailing in the DOS and to the progressive shift of the maximum in $D(E)$ as ρ is increased into the upper half of the band. The parallel consequences of screening for the localization characteristics of the system will be discussed further in the next section.

Finally, in Fig. 4 we compare the computed DOS with that resulting from a substitutionally disordered system in which active sites are distributed randomly on an underlying fcc lattice, as studied by Ching and Huber.[20(a)] In each case $N=1016$ and $n_{\rm con}=6$. The hard-sphere diameter is related to the fcc lattice constant l by $\sigma=l/\sqrt{2}$ (the spheres touch when close packed). $\rho^*=0.01$ in both calculations, and the ratio $\sigma/a_H=0.9$ is also fixed. From the figure we see that towards the upper end of the band a noticeable structure appears in the lattice-based $D(\tilde{E})$. This is to be expected if the region is dominated by interaction between neighboring or near-neighboring sites, as the discrete structure of the lattice will be most evident on small length scales. In particular, the nearest-neighbor distance for sites on an fcc lattice is $l/\sqrt{2}=\sigma$, and nearest-neighbor pair states give rise to an (antibonding) energy of $\exp(-\sigma/a_H)=0.406$. A strong peak in the lattice-based $D(\tilde{E})$ at this energy is clearly evident.

III. LOCALIZATION

From the eigenvector coefficients $\{C_{i\alpha}\}$ obtained as described in Sec. II, we form the IPR, L_α, given by[24]

$$L_\alpha=\sum_i |C_{i,\alpha}|^4 . \tag{12}$$

L_α is unity for an eigenstate α localized entirely on a single site ($C_{i,\alpha}=\delta_{ij}$), and $L_\alpha=n^{-1}$ for a state uniformly spread over n sites ($C_{i,\alpha}=n^{-1/2}$, $i=1-n$). In an infinite system, therefore, extended states have $L_\alpha=0$, and localized states are characterized by a finite L_α. Further, in an infinite system localized and extended states cannot coexist at the same energy:[32] The L_α are distributed such that L_α is zero for states in the range $E_c^-<E_\alpha<E_c^+$ and is finite for states outside this range, where $E_c^\pm$ are the upper and lower mobility edges. In a finite system these distinctions are blurred, and in attempting to infer mobility edges from the IPR there are two related problems to face. First, one must choose an appropriate cutoff in L_α to serve as a lower bound on localized states. And second, even if one can provide a reasonable estimate for the cutoff, the location of mobility edges will be uncertain due to the distribution of L_α's on the eigenenergy axis.

As pointed out by Thouless,[32] close to a mobility edge the wave function of an extended eigenstate is concentrated only on a small fraction of the sites, of order $\sim(r+1)^{-3}$, where r is about 2 or 3. If applicable to a finite system of N sites, this suggests[10(a)] the cutoff value $L_c=K/N$, where $K\approx 30-60$. Blumen *et al.*[18] chose a cutoff of 0.2 ($K=20$). In contrast, Ching and Huber[20(a)] chose $6/N$ (with $N=1000$), which has been criticized by Elyutin[10(a)] as being somewhat low. In this work, for $N=500$, we shall take a cutoff value of 0.16 ($K=80$): The time-dependent work on 500- particle systems discussed in Sec. IV at least shows this to be reasonable, and we believe 0.16 to be an adequate estimate of the cutoff.

The major problem in attempting to infer mobility edges from studies on a finite system is the distribution of L_α's on the energy axis: Within a given small energy range there will be a distribution of L_α's spreading above and below the chosen cutoff value. This is illustrated in Fig. 5 for $\rho^*=0.01$ (and $\sigma/a_H=0.9$), which shows a scatter plot of the L_α as a function of energy obtained from six configurations of 500 particles. The figure shows reasonable evidence for the existence of an upper mobility edge at around $\tilde{E}_c^+=0.07$, although the situation in

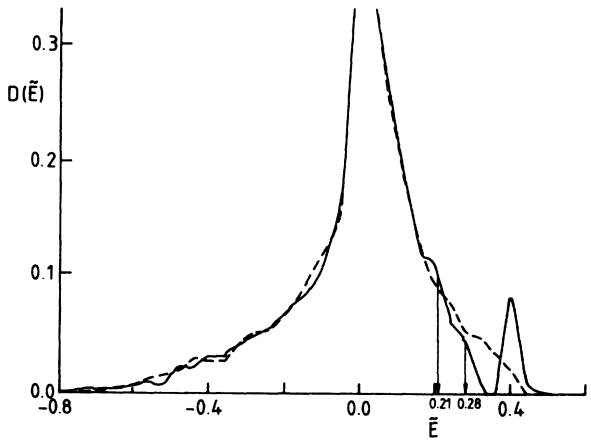

FIG. 4. A comparison between the DOS for the hard-sphere fluid (dashed line) and the randomly substituted fcc lattice (solid line) for $\rho^*=0.01$ and $\sigma/a_H=0.9$.

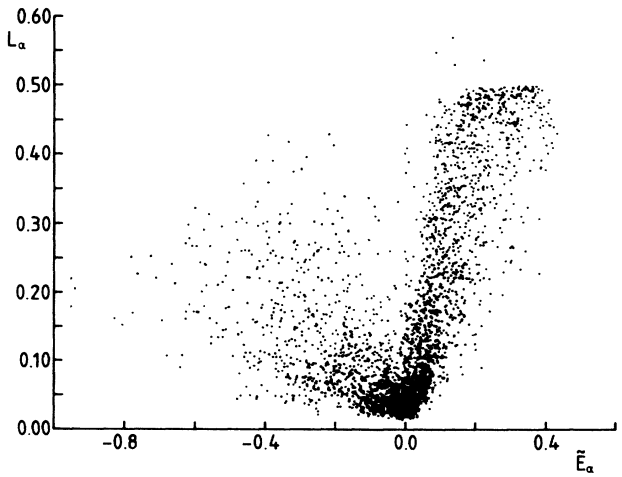

FIG. 5. A scatter plot of the IPR of an individual eigenstate L_α vs the eigenvalue E_α at $\rho^*=0.01$ and $\sigma/a_H=0.9$. The results from six configurations of 500 particles are shown.

regard to a lower mobility edge is obscure (even if we increase substantially the number of configurations). For $\tilde{E} \gtrsim 0.07$ the great majority of eigenstates are localized with an IPR greater than 0.16; similarly, for $-0.2 \lesssim \tilde{E} \lesssim 0.07$ the vast majority of eigenstates have an IPR less than 0.16 and are thus considered extended. For $\tilde{E} \lesssim -0.4$, there are more than twice as many eigenstates with $L_\alpha > 0.16$ than with $L_\alpha < L_c$, and for $-0.3 \lesssim \tilde{E} \lesssim -0.2$ the converse is true. A value of $\tilde{E}_c^-$ somewhere between -0.3 and -0.4 would not seem unreasonable, but the situation cannot be regarded as clear.

Assuming a belief of the incipient appearance of a lower mobility edge, however, we would like to assess qualitatively how the mobility edges vary with density [mobility-edge trajectories (MET's)]. We thus think it desirable to provide at least a rough estimate of the lower mobility edge. To this end we study the mean IPR. $\bar{L}_\alpha$, averaged over a small energy interval $\Delta\tilde{E}$ as described in Sec. II for the DOS. For an infinite system the mean IPR will be finite (zero) over an interval containing exclusively localized (extended) states; it will also be finite in an energy interval which includes a mobility edge, which is thus smeared out by an amount of order $\Delta\tilde{E}$. For a finite-sized system the resultant $\bar{L}_\alpha$ will always be nonzero and will clearly weight localized states more than those considered to be extended. Unless a given interval is heavily dominated by states which can be considered localized, we would expect a criterion to estimate mobility edges, which is based upon a given cutoff $\bar{L}_c$ to *overestimate* somewhat the range of localized states. Inspection of Fig. 5 suggests that we might, therefore, expect such a criterion to provide a reasonable estimate for the upper mobility edge and to underestimate the location of $|\tilde{E}_c^-|$.

In Fig. 6 we show the mean IPR corresponding to Fig. 5, but with a total of 12 configurations included in the statistics. With the cutoff criterion $\bar{L}_c = 0.16$ we estimate $\tilde{E}_c^+ = 0.07$ and $\tilde{E}_c^- \simeq -0.35$, which are compatible with the discussion of Fig. 5, although it is clear that states in the lower half-band with $\tilde{E} < \tilde{E}_c^-$ are only very weakly localized. Note too the rather sharp rise in the $\bar{L}_\alpha$ for $\tilde{E} > \tilde{E}_c^+$, to a value of around $\frac{1}{2}$ towards the edges of the band indicating the preponderance of antibonding pair states, as commensurate with the remarks made in Sec. II in connection with the DOS.

Figure 7 shows the system size dependence of the mean IPR for fixed $N \times n_{\text{con}} = 6000$ and for $N = 300$, 500, 1000, and 2000 particle systems. System size effects are, as one expects, particularly pronounced towards the band center where states are most delocalized, and are also evident, but progressively less so, at least for energies in the range $-0.4 \lesssim \tilde{E} < 0$.

To assess MET's we have obtained data from 12 configurations of 500 particles (with $\sigma/a_H = 0.9$) at some 15 different densities. Mobility edges at a given density are estimated using the criterion described above. Band-edge trajectories are also estimated by extrapolation of the DOS onto the energy axis. As is evident from the discussion in Sec. II (see also Figs. 1 and 3), this is a reasonable procedure for the upper band edge, and for the lower band edge it provides a useful rough guide to where the DOS vanishes. In Fig. 8 we plot the resultant band-edge and mobility-edge trajectories. It is clear from the figure that the upper band edge $\tilde{E}_+$ occurs at an energy which, over the density range studied, is only slightly greater than $\exp(-\sigma/a_H) \simeq 0.41$ (cf. Sec. II). The increasing asymmetry in the DOS as ρ is progressively increased is evident in the behavior of the lower band-edge trajectory. Parallel to the band-edge asymmetry, we see a pronounced asymmetry in the estimated MET's. In fact, Fig. 8 is qualitatively similar to Fig. 3 of Ref. 16, and the

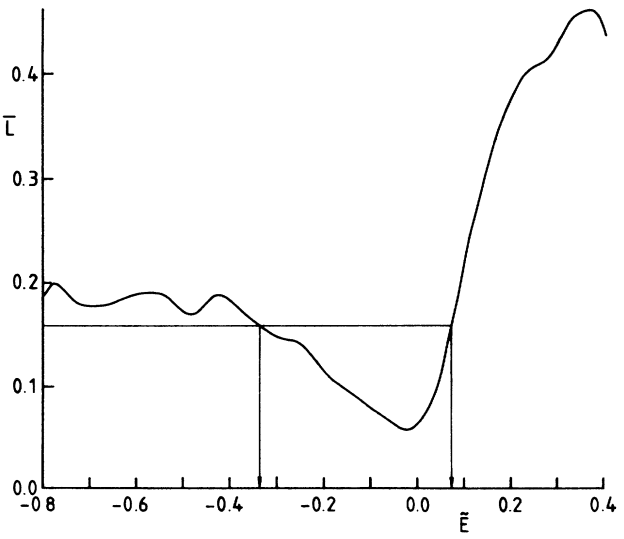

FIG. 6. The mean IPR ($\bar{L}$) vs energy for $\rho^* = 0.01$ and $\sigma/a_H = 0.9$ (12 configurations of 500 particles). The horizontal line shows the localization criterion $\bar{L}_c$ and the vertical arrows mark the mobility edge positions, according to this criterion.

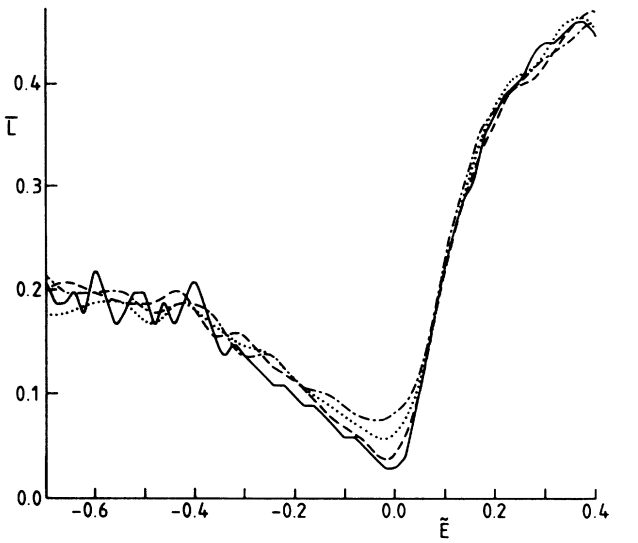

FIG. 7. The system size dependence of the mean IPR at $\rho^* = 0.01$ and $\sigma/a_H = 0.9$, the vertical lines show the mobility edges inferred from the 500-particle runs (Fig. 6). The solid line shows the results for 2000 particles (3 configurations); dashed line—1000 (6 configurations); dotted line—500 (12 configurations); dash-dotted—300 (20 configurations).

observed asymmetry in the MET's may also be understood physically in terms of screening, as introduced in Ref. 16 and described in Sec. II in relation to the DOS. Since for $\tilde{E}>0$ ($\tilde{E}<0$) the renormalized transfer-matrix element $\Phi_{ij}(E)$ [see Eq. (11)] is of shorter (longer) spatial range than the bare transfer-matrix element V_{ij}, we expect that for a given $|\tilde{E}|$ the critical density above which upper half-band states of energy $+\tilde{E}$ become extended will be greater than that for which lower half-band states at $-\tilde{E}$ become extended. This behavior is indeed apparent in Fig. 8. The existence of spatial antiscreening in the lower half-band implies that states in this region are much more susceptible to delocalization with decreasing disorder than are states in the upper half-band. We believe this to be a major factor responsible for the difficulty in locating accurately a lower mobility edge from finite-sized simulations.

In passing we would add that Puri and Odagaki[12(a)] and Fertis *et al.*[14] have also calculated band-edge and mobility-edge trajectories for a three-dimensional topologically disordered system with a (modified) exponential transfer-matrix element. The spatially disordered system was replaced by a pair of sites embedded in an effective medium, a homomorphic cluster coherent potential approximation was used to calculate the averaged Green's function for the system, and the localization of eigenstates was inferred from the $L(E)$ criterion.[33] In neither case was asymmetry observed in the MET's. This, however, is inevitable by construct: The effective medium is assumed to be a crystal lattice, and if the unperturbed Green's function for the arbitrarily chosen lattice is symmetric in E (as in Refs. 12 and 14) then asymmetry in the band-edge and mobility-edge trajectories is precluded.

From Fig. 8 we see that the Anderson transition density (at which the mobility edges coalesce) corresponds to $\rho_A^{1/3}a_H \simeq 0.18$ ($\sigma/a_H=0.9$). As discussed previously we expect this to be an overestimate. It is in reasonable agreement with Ref. 15(a) ($\rho_A^{1/3}a_H=0.14$ for $\sigma/a_H=0.9$), and with the work of Elyutin[10(a)] ($\rho_A^{1/3}a_H=0.17\pm0.02$ for $\sigma=0$), although it is considerably lower than $\rho_A^{1/3}a_H=0.37\pm0.08$ found for $\sigma=0$ by Ching and Huber.[20(a)] Elyutin[10(a)] points out, however, that Ching and Huber's results are in fact compatible with $\rho_A^{1/3}a_H \simeq 0.17$ if a higher L_α cutoff is applied to their IPR distributions. We have also investigated the effects of varying σ/a_H over the range 0.5–1.3. The effect on the band-edge trajectories is quite pronounced as is evident from the discussion of Sec. II, but the MET's in general, and the Anderson transition density in particular, are altered only to a minor extent. This is compatible with the analytical results of Ref. 15(a), where $\rho_A^{1/3}a_H$ is only weakly dependent on σ/a_H for $\sigma/a_H \lesssim 1.5$, and with the numerical calculations of Puri and Odagaki in Ref. 12(b) over the σ/a_H range studied here.

We now discuss briefly a measure of the spatial extent of the eigenstates. Following Yonezawa[13] we define an effective "radius of gyration," R_α, of an eigenstate α, by

$$R_\alpha^2=\tfrac{1}{3}(R_{\alpha x}^2+R_{\alpha y}^2+R_{\alpha z}^2)\ , \tag{13}$$

where $R_{\alpha x}^2=\overline{x^2}-\bar{x}^2$, etc. and

$$\overline{x^2}=\sum_i |C_{i,\alpha}|^2(R_{i_x}-R_{o_x})_{\min}^2\ ,$$

$$\bar{x}=\sum_i |C_{i,\alpha}|^2(R_{i_x}-R_{o_x})_{\min}\ . \tag{14}$$

Here, R_{i_x} denotes the x coordinate of site i and site o is the site with maximum amplitude in the given eigenstate; a subscript min implies that a minimum image convention was applied to all distances. In Fig. 9 we show a scatter plot of $(R_\alpha/L)^2$ against $\tilde{E}_\alpha$, where L is the cell length, for a reduced density $\rho^*=0.01$ and for a single configuration of a 500-particle system. States in the vicinity of the band center $\tilde{E}=0$ typically have $R_\alpha > \frac{1}{3}L$ and therefore occupy an appreciable fraction of the volume of the system as is compatible with the behavior of extended states. As we move progressively away from

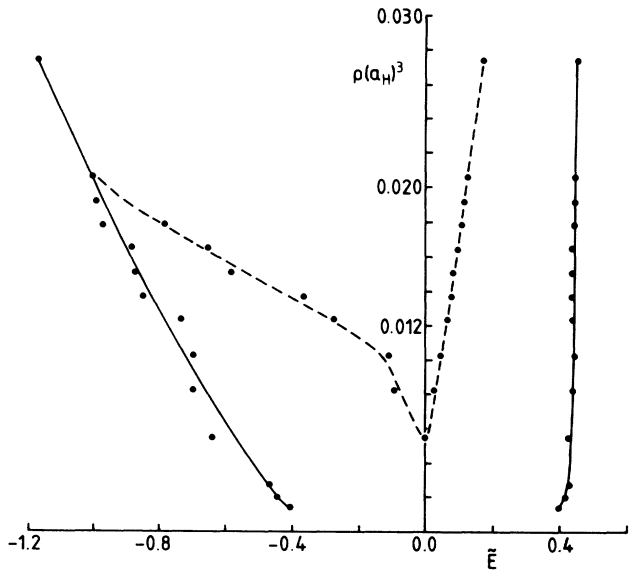

FIG. 8. Band-edge and mobility-edge (using $\bar{L}_c=0.16$) trajectories for $\sigma/a_H=0.9$. The lines are simply aids to the eye, the solid one shows the band edge and the dashed the mobility edge.

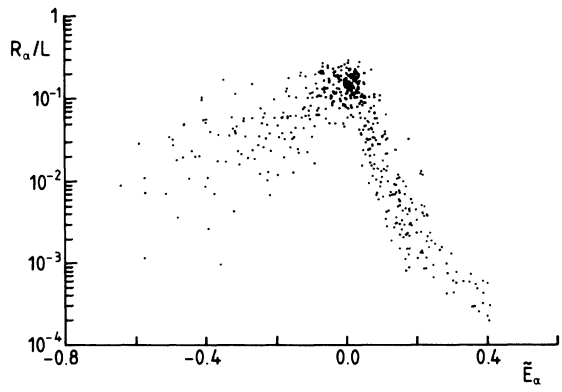

FIG. 9. A scatter plot of the radius of gyration, i.e., R_α/L, vs eigenvalue $\tilde{E}_\alpha$ for a single configuration of 500 particles at $\rho^*=0.01$ and $\sigma/a_H=0.9$.

the band center, R_α/L clearly drops off. The drop is most pronounced in the upper half-band: For $\tilde{E}>0.07$, R_α/L declines rapidly from a value of ~ 0.2 at $\tilde{E}\simeq 0.07$ to a typical value of ~ 0.03 at $\tilde{E}=0.2$ and to values as low as $R_\alpha/L\simeq 0.01$ at the upper edge of the band. There is clearly evidence for the dominance of states which could be considered as localized in the upper half of the band, in agreement with the preceding discussion. There is also an evident diminuation in R_α/L as one moves to the lower edge of the band, but the drop is less pronounced than in the upper portion, and the scatter rather wide: This is compatible with our previous remarks on the difficulty of locating a lower mobility edge.

In a finite-size system, the spatial extent of states considered as extended will clearly be controlled by the size of the simulation cell. For the fixed density $\rho^*=N(\sigma/L)^3=0.01$, we have, therefore, examined the system size dependence of $\bar{R}_\alpha$, the mean value of R_α for eigenstates α with energies in the small interval from $\tilde{E}=0$ to $\tilde{E}=0.01$, for fixed $Nn_{\rm con}=6000$ and for $N=100$, 200, 300, 500, and 1000 particle systems. As N (and thus L) is progressively increased, we find as expected that $\bar{R}_\alpha$ increases. For $\rho^*=0.01$, significant system size effects are evident for $N=100$–300. It appears, however, that $\bar{R}_\alpha$ saturates to a value of $\sim 0.42L$ for N in excess of 500, and thus that $\bar{R}_\alpha \propto L$ as $L\to\infty$, as one might expect for truly extended eigenstates.

IV. TIME-DEPENDENT BEHAVIOR

Consider a given realization of the system, and suppose that at time $t=0$ an excitation is created on a specific site i. The subsequent time evolution of the excitation is described by the Schrödinger equation

$$i\hbar\frac{\partial}{\partial t}|\Psi(t)\rangle=\hat{\mathcal{H}}|\Psi(t)\rangle\ , \tag{15}$$

where $\hat{\mathcal{H}}$ is given by Eq. (1). The time-dependent wave function can be expanded in terms of the site basis $\{|j\rangle\}$

$$|\Psi(t)\rangle=\sum_j a_j^i(t)|j\rangle\ , \tag{16}$$

where $a_j^i(t)$ is the probability amplitude that the excitation will be found on site j at time t given that it was located on i at $t=0$ [$a_j^i(0)=\delta_{ji}$]. The wave function may also be expanded as

$$|\Psi(t)\rangle=\sum_\alpha b_\alpha|\Psi_\alpha(t)\rangle\ ,$$

where

$$|\Psi_\alpha(t)\rangle=\exp(-iE_\alpha t/\hbar)|\Psi_\alpha(0)\rangle$$

is a stationary state of the tight-binding Hamiltonian with energy E_α. It follows from Eqs. (3a) and (16) that $b_\alpha\equiv\langle\Psi_\alpha(t)|\Psi(0)\rangle=C_{i,\alpha}^*$, so that

$$|\Psi(t)\rangle=\sum_\alpha C_{i,\alpha}^*|\Psi_\alpha\rangle\exp(-iE_\alpha t/\hbar) \tag{17}$$

and

$$a_j^i(t)=\sum_\alpha C_{j,\alpha}C_{i,\alpha}^*\exp(-iE_\alpha t/\hbar)\ . \tag{18}$$

The probability $P_{ii}(t)=|a_i^i(t)|^2$ that the excitation will be found on site i at time t, given that it was located there at $t=0$, is thus given by

$$P_{ii}(t)=\sum_{\alpha,\beta}|C_{i,\alpha}|^2|C_{i,\beta}|^2\cos(\Delta\tilde{E}_{\alpha\beta}\tau)\ . \tag{19}$$

$\Delta\tilde{E}_{\alpha\beta}=\tilde{E}_\alpha-\tilde{E}_\beta$ and $\tau=V_0t/\hbar$ are a dimensionless energy difference and time, respectively. The ensemble-averaged probability that an excitation will be found at time t on the same site which it is located at $t=0$ is given by:

$$\bar{P}(t)=\left\langle\frac{1}{N}\sum_i P_{ii}(t)\right\rangle\ . \tag{20}$$

From a calculation of the eigenvalues and eigenvector coefficients of the tight-binding Hamiltonian, as described in the preceding sections, we can thus calculate $P_{ii}(t)$ and $\bar{P}(t)$. A good deal of information can be extracted from such studies, but we focus here on the behavior of $P_{ii}(t)$ and $\bar{P}(t)$ in relation to the localized or extended nature of the eigenstates of the system.

In Fig. 10 we show the calculated $\bar{P}(\tau)$ as a function of time τ, obtained from data on two configurations of $N=500$ particles. The upper curve is for a reduced density $\rho^*=0.01$ ($\rho a_H^3\simeq 0.014$) and the lower is for $\rho^*=0.05$ ($\rho a_H^3\simeq 0.069$). Note that $\bar{P}(\tau)$ decays much more rapidly at short times as density as increased, but that both curves continue to exhibit decay over a much longer timescale than that characteristic of the initial drop. The short time decay of $P_{ii}(\tau)$ reflects the ability of an excitation to explore its immediate local environment. It is determined mainly by the energetic range of the eigenstates which overlap spatially the initial site and is not greatly affected by the localized or extended nature of these states. This can be seen by noting that the coefficient of τ^2 in a short time expansion of

$$P_{ii}(\tau)=1-\gamma\tau^2+O(\tau^4)$$

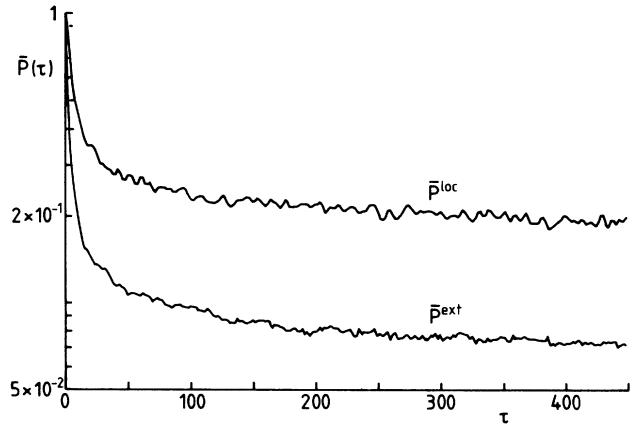

FIG. 10. $\bar{P}(\tau)$ vs τ, the lower curve is for a density of $\rho\sigma^3=0.01$ and the upper for $\rho\sigma^3=0.05$. The data are obtained from two configurations of 500 particles with $\sigma/a_H=0.9$.

is given by

$$\int (\tilde{E}-\bar{\tilde{E}})^2 N_i(\tilde{E})d\tilde{E} ,$$

where

$$\bar{\tilde{E}}=\int \tilde{E}N_i(\tilde{E})d\tilde{E}$$

and

$$N_i(\tilde{E})=\sum_\alpha |C_{i,\alpha}|^2\delta(\tilde{E}-\tilde{E}_\alpha)$$

is the local density of states which overlap with site i, the ensemble average of which is $D(\tilde{E})$. The increasingly rapid short time decay of $\bar{P}(\tau)$ with increasing density is thus primarily due to the effects of band broadening.

In contrast, it is evident that the long time decays in $\bar{P}(t)$ reflect the existence of eigenstates overlapping the initial site which occupy an appreciable volume of the system and which can, therefore, be considered as extended. An excitation created at $t=0$ on site i has a finite probability $|C_{i,\alpha}|^2$ [see Eq. (17)] of being initially in any eigenstate which overlaps the site. The overall time evolution of $P_{ii}(\tau)$ thus ultimately reflects the ability of the excitation to explore the regions of space associated with these eigenstates. We would expect the contribution to $P_{ii}(\tau)$ arising from eigenstates which occupy a small volume of space to decay rapidly to the infinite time contribution to P_{ii} arising from such states. And we would expect the contributions to $P_{ii}(\tau)$ arising from extended eigenstates to decay more slowly to its infinite-time value, reflecting the greater time required for an excitation in such states to explore the volume occupied by them. To point this up we first separate $P_{ii}(t)$ as

$$P_{ii}(t)=\sum_\alpha |C_{i,\alpha}|^4+\sum_{\alpha,\beta}{}' |C_{i,\alpha}|^2|C_{i,\beta}|^2\cos(\Delta\tilde{E}_{\alpha\beta}\tau) , \tag{21}$$

where a prime denotes $\beta\neq\alpha$. The first term on the right-hand side of Eq. (21) is simply the infinite time value, $P_{ii}(\infty)$, of $P_{ii}(\tau)$, see, e.g., Refs. 15(b) and 32 [note too that $\bar{P}(\infty)$ is simply an ensemble average of the mean IPR of the entire band]. In the limit of an infinite system, $P_{ii}(\infty)=0$ if no localized eigenstates overlap site i and is nonzero if (any) localized states overlap with the site. In contrast, $P_{ii}(\infty)$ is inevitably nonzero for a finite-size system. However the function $\delta P_{ii}(\tau)=P_{ii}(\tau)-P_{ii}(\infty)$, given by

$$\delta P_{ii}(t)=\sum_{\alpha,\beta}{}' |C_{i,\alpha}|^2|C_{i,\beta}|^2\cos(\Delta\tilde{E}_{\alpha\beta}\tau) \tag{22}$$

describes the decay of $P_{ii}(t)$ to its infinite time value, and vanishes as $\tau\rightarrow\infty$ by definition. The separation $\Delta\tilde{E}_{\min}$ between energetically adjacent eigenstates of the system is of order $\Delta\tilde{E}_{\min}\sim B/V_0N$, where B is the bandwidth of $D(E)$ at the chosen density. The maximum time scale τ_m over which we might expect to observe decay in $\delta P_{ii}(\tau)$ [or $\bar{P}(\tau)$] is of order $1/\Delta\tilde{E}_{\min}$. For our $N=500$ particle systems we see from Fig. 8 that $B/V_0\sim 1-2$ for densities in the range of interest; thus $\tau_m\sim 250-500$, and decays in $\bar{P}(\tau)$ over such long times are evident in Fig. 10 (see also Figs. 11–13). We would, however, argue that localized eigenstates cannot contribute to these long decays. This is essentially because localized states can coexist in a very narrow energy interval only if they are spatially well separated. In consequence, if the coefficient $C_{i,\alpha}$ of atom i in eigenstate α is appreciable, the coefficient $C_{i,\beta}$ of the same atom in a localized eigenstate β with energy very close to that of α is exponentially smaller than $C_{i,\alpha}$.

To see this, suppose we have localized eigenstate α with energy $\tilde{E}_\alpha$, centered with maximum amplitude on site i, and with a wave function of form $\Psi_\alpha(r)\sim\exp(-r/\xi)$, where ξ is a localization length. Consider another exponentially localized eigenstate β with energy $\tilde{E}_\beta\simeq\tilde{E}_\alpha+\Delta\tilde{E}_{\min}$ centered on a site a distance R away from site i. We ask for $|C_{i,\beta}|^2$ the squared coefficient of site i in the eigenstate β. Following Mott and Kaveh,[34] we argue that the magnitude of the transfer integral between these two states must be less than about $\frac{1}{2}\Delta E_{\min}$, if the splitting is not to take them out of the range $\Delta E_{\min}$. This, however, imposes a minimum spatial separation, $R_{\min}$, between states α and β, and $|C_{i,\beta}|^2$ will be exponentially smaller than $|C_{i,\alpha}|^2$ by a factor less than $\sim\exp(-2R_{\min}/\xi)$. We take the transfer integral to be[34] $-V_0\exp(-R/\xi)$, and with $(\Delta\tilde{E}_{\min})^{-1}\simeq 250-500$ as above, it follows than $R_{\min}/\xi\gtrsim 6-7$. $|C_{i,\beta}|^2$ is thus exponentially smaller than $|C_{i,\alpha}|^2$ by a factor less than $\sim e^{-12}-e^{-14}$. Localized states give an exponentially small contribution to $\delta P_{ii}(\tau)$ on timescales of the order of τ_m. The long time decays in $\bar{P}(\tau)$ are, as intuition would suggest, due to states which can be considered as extended and which are able to coexist in a region which is small both energetically and spatially.

The question we wish to address here is what value of L_α constitutes an acceptable cutoff between localized and extended states in our finite-size simulations? To investigate this we define

$$P_{ii}^{\rm loc}(t)=\sum_{\substack{\alpha,\beta\\ L>L_c}} |C_{i,\alpha}|^2|C_{i,\beta}|^2\cos(\Delta\tilde{E}_{\alpha\beta}\tau) , \tag{23a}$$

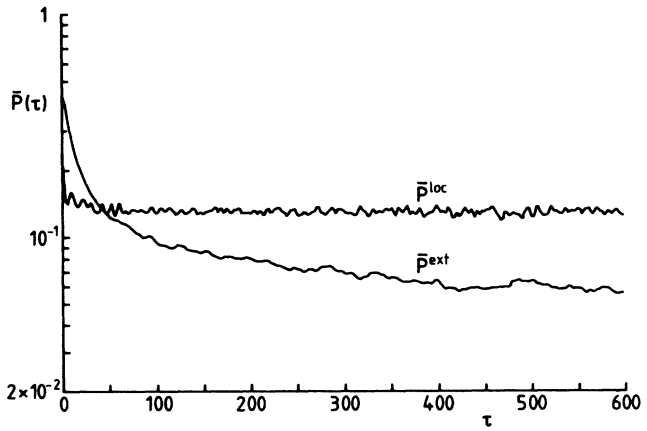

FIG. 11. $\bar{P}^{\rm ext}(\tau)$ and $\bar{P}^{\rm loc}(\tau)$ vs time τ [Eqs. (23a) and (23b)] using the cutoff criterion $\bar{L}_c=0.16$. Results from two configurations of 500 particles with $\rho\sigma^3=0.01$ and $\sigma/a_H=0.9$ are shown.

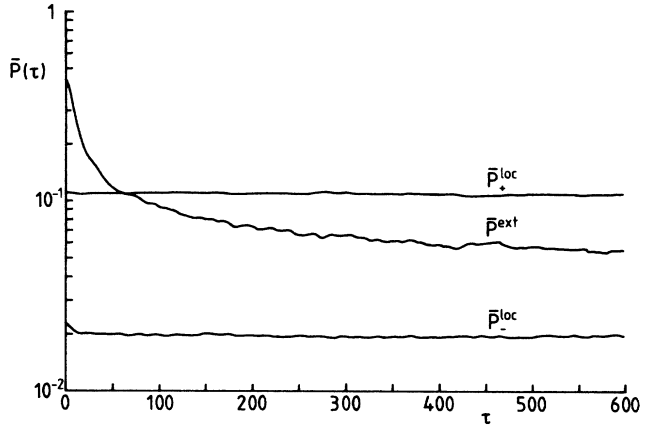

FIG. 12. $\bar{P}^{loc}$ is shown further resolved into separate contributions from the upper ($\bar{P}_+$) and lower ($\bar{P}_-$) half-bands together with $\bar{P}^{ext}$. For $\rho^*=0.01$ and $\sigma/a_H=0.9$ ($\rho a_H^3=0.014$), data from 12 configurations of 500 particles are shown.

$$P_{ii}^{ext}(t)=\sum_{\substack{\alpha,\beta \\ L<L_c}} |C_{i,\alpha}|^2 |C_{i,\beta}|^2 \cos(\Delta\tilde{E}_{\alpha\beta}\tau) , \qquad (23b)$$

where the sums are restricted to $L>L_c$ or $L<L_c$ as appropriate. Note that, by construct, $P_{ii}(\tau)\neq P_{ii}^{loc}(\tau)+P_{ii}^{ext}(\tau)$ except as $\tau\rightarrow\infty$. We search for that value of L_c such that if a close but lower cutoff is used in each of the sums in Eq. (23), then both $\bar{P}^{ext}(\tau)$ and $\bar{P}^{loc}(\tau)$ exhibit decays over a timescale of order τ_m, indicating that states which we would consider as extended are included in both functions.

By investigation of this problem over a wide range of densities in our 500 particle simulations, we find that $L_c=0.16$ constitutes an appropriate cutoff. As an initial illustration we show in Fig. 11 $\bar{P}^{ext}(\tau)$ and $\bar{P}^{loc}(\tau)$ as a function of time τ for the density $\rho a_H^3\simeq 0.014$ ($\rho^*=0.01$), and with the cutoff $L_c=0.16$. The long time decay in $\bar{P}^{ext}(\tau)$ is clear; in contrast, although oscillating in nature as discussed below, $\bar{P}^{loc}(\tau)$ decays to its infinite time value on a much shorter timescale. If a cutoff significantly lower than $L_c=0.16$ is employed, we find that markedly long time decays appear in $\bar{P}^{loc}(\tau)$: This is certainly the case with a cutoff in L less than ~ 0.14–0.15. The oscillatory behavior of $\bar{P}^{loc}(\tau)$ is mainly due to interference between localized states in the upper half-band and localized states in the lower portion of the band. To demonstrate this we further define $\bar{P}_+^{loc}(\tau)$ and $\bar{P}_-^{loc}(\tau)$, where $+(-)$ denotes that the eigenstates α and β in the sum (23a) are further restricted to $\tilde{E}_\alpha$ and $\tilde{E}_\beta$ greater (less) then zero, in addition to the $L>L_c=0.16$ constraint. Interference effects between localized states in the upper and lower regions of the band are thus excluded. In Fig. 12 we plot the resultant $\bar{P}_\pm^{loc}(\tau)$ and $\bar{P}^{ext}(\tau)$, for the same density as in Fig. 11. The oscillatory behavior apparent in Fig. 11 for $\bar{P}^{loc}(\tau)$ is now absent, and both $\bar{P}_+^{loc}(\tau)$ and $\bar{P}_-^{loc}(\tau)$ decay very rapidly to their infinite time values [which satisfy $\bar{P}_+^{loc}(\infty)+\bar{P}_-^{loc}(\infty)=\bar{P}^{loc}(\infty)$]. $\bar{P}_-^{loc}(\tau)$ decays on a timescale τ of order 10, and $\bar{P}_+^{loc}(\tau)$ decays on an even shorter timescale which is not resolved on the scale of the figure. We find again that if a cutoff significantly lower than $L_c=0.16$ is employed, markedly long time decays appear in $\bar{P}_+^{loc}$ and $\bar{P}_-^{loc}(\tau)$. Finally, to demonstrate that the above behavior is not peculiar to $\rho a_H^3=0.014$, we plot in Fig. 13 the functions $\bar{P}_\pm^{loc}(\tau)$ and $\bar{P}^{ext}(\tau)$ for a higher density ($\rho a_H^3=0.024$) and a lower density ($\rho a_H^3=0.008$). In both cases the time decay patterns are similar in character to those associated with the intermediate density studied in Figs. 11 and 12.

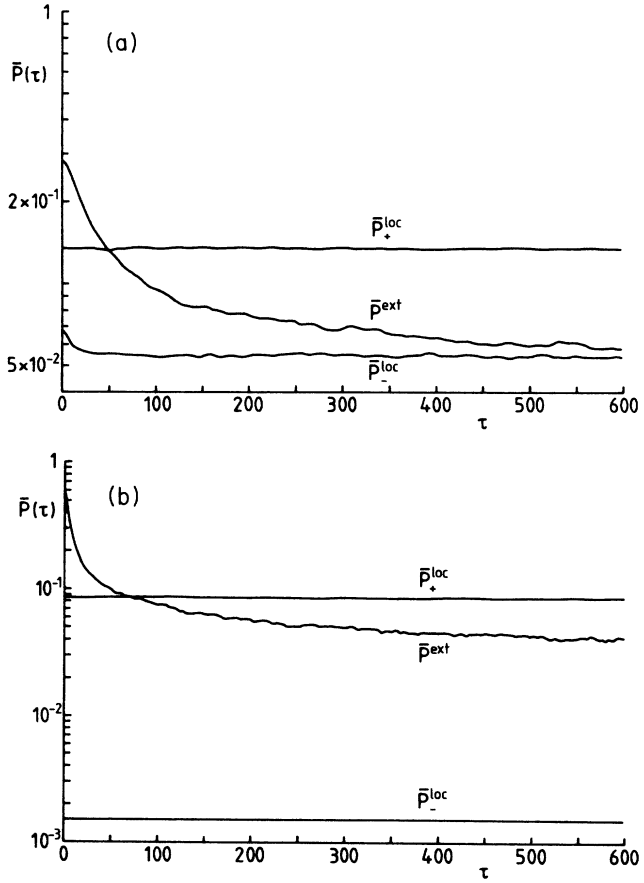

FIG. 13. As Fig. 12 but for densities of $\rho a_H^3=0.08$ and 0.024 [Eqs. (13a) and (13b), respectively].

We believe the above results show that for 500-particle systems a cutoff of $L_c=0.16$ is at least a reasonable boundary between localized and extended states, although the problem of locating mobility edges is obviously not ameliorated for the reasons described in Sec. III. In subsequent work we shall discuss additional information which can be extracted from time-dependent studies.

ACKNOWLEDGMENT

We are grateful to Julia Carter for assistance in the early stages of the calculations.

[1]P. W. Anderson, Phys. Rev. **109**, 1492 (1958).
[2]*Anderson Localization,* edited by Y. Nagaoka and H. Fukuyama (Springer, Berlin, 1982).
[3]*The Metal Nonmetal Transition in Disordered Systems,* edited by L. R. Friedman and D. P. Tunstall (Scottish Universities Summer School in Physics, Edinburgh, 1978).
[4]N. F. Mott, *Metal Insulator Transitions* (Taylor and Francis, London, 1974).
[5]J. Klafter and J. Jortner, J. Chem. Phys. **71**, 2210 (1979).
[6]A. H. Francis and R. Kopelman, in *Laser Spectroscopy of Solids,* edited by W. M. Yen and P. M. Selzer (Springer, Berlin, 1981).
[7]K. S. Schweizer, J. Chem. Phys. **85**, 4638 (1986).
[8]D. E. Logan and P. G. Wolynes, Phys. Rev. B **29**, 6560 (1984).
[9]L. Fleishman and D. L. Stein, J. Phys. C **12**, 4817 (1979).
[10](a) P. V. Elyutin, J. Phys. C **16**, 4151 (1983); (b) Fiz. Tverd. Tela (Leningrad) **21**, 2765 (1979) [Sov. Phys.—Solid State **21**, 1590 (1979)].
[11]T. Odagaki, Solid State Commun. **33**, 861 (1981).
[12](a) A. Puri and T. Odagaki, Phys. Rev. B **24**, 5541 (1981); (b) **29**, 1707 (1984).
[13]F. Yonezawa, J. Non-Cryst. Solids **35/36**, 29 (1980).
[14]A. C. Fertis, A. N. Andriotis, and E. N. Economou, Phys. Rev. B **24**, 5806 (1981).
[15](a) D. E. Logan and P. G. Wolynes, Phys. Rev. B **31**, 2437 (1985); (b) **36**, 4135 (1987).
[16]D. E. Logan and P. G. Wolynes, J. Chem. Phys. **85**, 937 (1986).
[17]L. J. Root, J. D. Bauer, and J. L. Skinner (unpublished).
[18]A. Blumen, J. P. Lemaistre, and I. Mathlouthi, J. Chem. Phys. **81**, 4610 (1984).
[19]J. P. Lemaistre and A. Blumen, Chem. Phys. Lett. **99**, 291 (1983).
[20](a) W. Y. Ching and D. L. Huber, Phys. Rev. B **25**, 1096 (1982); (b) **26**, 5596 (1982).
[21]M. Kikuchi, J. Phys. Soc. Jpn. **37**, 904 (1974); **41**, 1459 (1976).
[22]B. T. Debney, J. Phys. C **10**, 4719 (1977).
[23]E. Abrahams, P. W. Anderson, D. C. Licciardello, and T. V. Ramakrishnan, Phys. Rev. Lett. **42**, 673 (1979).
[24]R. J. Bell and P. Dean, Discuss. Faraday Soc. **50**, 55 (1970).
[25]T. Matsubara and Y. Toyozawa, Prog. Theor. Phys. **26**, 739 (1961).
[26]F. Cryot-Lackmann and J. P. Gaspard, J. Phys. C **7**, 1829 (1974).
[27]G. Aoki and H. Kamimura, J. Phys. Soc. Jpn. **40**, 6 (1976).
[28]R. Osorio, N. Majlis, and K. A. Chao, J. Phys. C **11**, 2779 (1978).
[29]I. Katz and S. A. Rice, J. Phys. C **5**, 1165 (1972).
[30]P. V. Elyutin, J. Phys. C **14**, 1435 (1981).
[31]E. Feenberg, Phys. Rev. **74**, 206 (1948).
[32]D. J. Thouless, Phys. Rep. **13**, 93 (1974).
[33]E. N. Economou and M. H. Cohen, Phys. Rev. B **5**, 2931 (1972).
[34]N. F. Mott and M. Kaveh, Adv. Phys. **3**, 329 (1985).